

Crystal structure and DFT studies of 4-(1-benzyl-5-methyl-1H-1,2,3-triazol-4-yl)-6-phenylpyrimidin-2-amine

S Murugavel^{1*}, S Vijayakumar², Sangaraiah Nagarajan³ & Alagusundaram Ponnuswamy³

¹Thanthai Periyar Government Institute of Technology, Vellore 632 002, India

²Department of Physics, Sri Balaji Chokkalingam Engineering College, Arni, Thiruvannamalai 632 317, India

³Department of Organic Chemistry, School of Chemistry, Madurai Kamaraj University, Madurai 625 021, India

Received 14 October 2014; accepted 16 June 2015

The title compound (1) 4-(1-benzyl-5-methyl-1H-1,2,3-triazol-4-yl)-6-phenylpyrimidin-2-amine (C₂₀H₁₈N₆) was synthesized and structurally characterized by elemental analysis, ¹H NMR, ¹³C NMR and single crystal X-ray diffraction. The compound crystallizes as a colourless needle shaped in the monoclinic system, space group C 2/c with cell constants: $a = 18.6636(6)$ Å, $b = 9.8655(4)$ Å, $c = 19.5249(7)$ Å, $\alpha = \gamma = 90.0^\circ$, $\beta = 107.900(2)^\circ$, $V = 3421.0(2)$ Å³, $Z = 8$. The molecular conformation is stabilized by an intra-molecular C—H...N hydrogen bond, which generates an S(6) ring motif. In the crystal, molecules are linked into one-dimensional infinite chains along *c*-axis by N—H...N hydrogen bond and C—H... π interactions involving the benzene ring attached to the triazole ring as an acceptor. These chains are alternately connected along *a*-axis by centro-symmetrically π — π interactions [ring centroid (triazole) ring centroid (pyrimidine) distance = 3.721 (1) Å and ring centroid (pyrimidine)...ring centroid (benzene ring attached to pyrimidine ring) distance = 3.825 (1) Å] forming a two-dimensional supra molecular network. The molecular geometry was also optimized using density functional theory using (DFT/B3LYP) method with the 6-311G(d,p) basis set and compared with the experimental data. Mulliken population analyses on atomic charges and HOMO-LUMO energy levels of the title compound have been calculated. The charge energy distribution and site of chemical reactivity of molecules were obtained by mapping electron density iso-surface with electrostatic potential surfaces. The thermo dynamical properties of the title compound at different temperature have been calculated and corresponding relations between the properties and temperature have also been obtained.

Keywords: X-ray structure determination, Hydrogen bond, Density functional theory, HOMO-LUMO energy level

1 Introduction

1,2,3-triazoles have found a wide range of important applications in the pharmaceutical, polymer, and material fields¹. In addition, they have shown a broad spectrum of biological properties such as anti-bacterial², anti-allergic³, anti-HIV activity⁴ and also serve as potential chemotherapeutic agents for various diseases⁵. On the other hand, substituted pyrimidine nuclei are found antiviral⁶, anti-tubercular, anti-neoplastic, anti-inflammatory, diuretic, anti-malarial and cardiovascular⁷. In view of these bioactivities of the individual heterocycles, it was envisaged that the synthesis of novel hybrid molecules containing two of the above said moieties in a single frame is worth the attempt. Literature survey reveals that so far there is no experimental and theoretical study for the title compound. In recent years, density functional theory (DFT) has become an increasingly useful tool for theoretical studies.

The success of DFT is mainly due to the fact that it describes small molecules more reliably than Hartree-Fock theory. It is also computationally less demanding than wave function based methods with inclusion of electron correlation^{8,9}. Thus, in order to characterize the correlation between molecular structure and macroscopic properties in the studied compound, it seems to be essential to undertake a detailed comparative study of the isolated molecule and the solid state unit. In this paper, a concerted approach by X-ray crystallography and DFT calculation is used, which takes advantage of both the high interpretative power of the theoretical studies and the precision and reliability of the experimental method.

The title compound has been synthesized and antibacterial activities are reported by Nagarajan *et al.*¹⁰. In this paper, synthesis and crystal structure of 4-(1-benzyl-5-methyl-1H-1,2,3-triazol-4-yl)-6-phenylpyrimidin-2-amine (C₂₀H₁₈N₆) is reported as well as theoretical studies using the DFT(B3LYP) method

*Corresponding author (E-mail: smurugavel27@gmail.com)

and 6-311G(d,p) basis set. The aim of the present work was to describe and characterize the molecular structure and some electronic structure properties of the title compound, both experimentally and theoretically. Also, comparison was made between experimental and calculated values.

2 Experimental and Computational Methods

2.1 Synthesis of title compound

The title compound (1) was obtained according to the reaction scheme in Fig. 1. A mixture of (E)-1-(1-benzyl-5-methyl-1H-1,2,3-triazol-4-yl)-3-phenylprop-2-en-1-one (0.2 g, 0.65 mmol), guanidine hydrochloride (0.18 g, 1.88 mmol) and NaOH (0.05 g, 1.25 mmol) in ethanol (10 mL) was refluxed for 40 min. Then, the reaction mixture was poured onto excess crushed ice and neutralized with dilute hydrochloric acid. The precipitated 4-(1-benzyl-5-methyl-1H-1,2,3-triazol-4-yl)-6-phenylpyrimidin-2-amine was filtered and re-crystallized from ethanol¹⁰. Needle like colourless single crystals of the title compound used in X-ray diffraction studies were grown in an ethanolic solution by slow evaporation of the solvent at room temperature and collected 82% yield.

The nuclear magnetic resonance spectra (¹H NMR and ¹³C NMR) were recorded in CDCl₃ and DMSO-d₆ on Bruker Advance 300 MHz spectrometer and the chemical shifts were reported as δ values in parts per million (ppm) relative to tetramethylsilane, with *J* values in Hertz. The splitting patterns in ¹H NMR spectra are reported as: s = singlet; d = doublet; br s = broad singlet; br d = broad doublet; and m = multiplet. ¹³C NMR data are reported with the solvent peak (CDCl₃ = 77.0 MHz) as the internal standard.

White solid: m.p. 152°C, yield 82%; IR (KBr): ν 3411, 3192, 1677, 1552, 1462, 1355, 1181, 834, 729, 700 cm⁻¹; ¹H NMR (300 MHz, CDCl₃): δ 8.12-8.09 (2H, m, ArH), 7.98 (1H, s, =CH), 7.49-7.18 (8H, m, ArH), 5.56 (2H, s, C₆H₅-CH₂), 5.07 (2H, brs, NH₂), 2.62 (3H, s, CH₃); ¹³C NMR (75 MHz, CDCl₃): δ 165.87, 163.14, 160.56, 142.30, 137.57, 134.51, 134.00, 133.94, 130.48, 130.42, 129.06, 128.71, 128.66, 128.41, 127.17, 104.50, 51.80, 9.82. MS

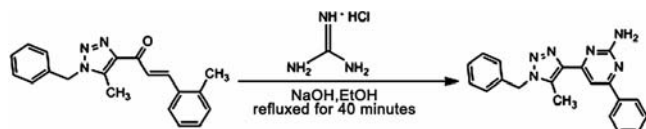


Fig. 1 — Synthesis of 4-(1-benzyl-5-methyl-1H-1,2,3-triazol-4-yl)-6-phenylpyrimidin-2-amine

(ESI): *m/z* (%) 343.33 (M + H); Anal. Calcd. for C₂₀H₁₈N₆: C, 70.16; H, 5.30; N, 24.54 Found: C, 70.09; H, 5.32; N, 24.50.

2.2 X-ray crystallography

A crystal of the title compound having approximate dimension 0.30×0.25×0.11 mm³ was mounted on a glass fiber using cyanoacrylate adhesive. All measurement were made on a Bruker AXS Kappa Apex II single crystal X-ray diffractometer using graphite mono-chromated MoK α (λ = 0.71071 Å) radiation and CCD detector. Diffraction data were collected at room temperature by the ω -scan technique. Accurate unit cell parameters and orientation matrix were obtained by a least-squares fit of several high angle reflections in the ranges 2.19° < θ < 28.96° for the title compound. The unit cell parameters were determined for 36 frames measured (0.5° phi-scan) from three different crystallographic zones and using the method of difference vectors. The intensity data were collected with an average four-fold redundancy per reflection and optimum resolution (0.75 Å). The intensity data collection, frames integration, Lorentz-polarization correction and decay correction were done using SAINT-NT (version 7.06a) software. Empirical absorption correction (multi-scan) was performed using SADABS¹¹ program. The structure was solved by direct methods using SHELXS-97 implemented in WinGX¹² program suit. The refinement was carried out by full-matrix least-square method on the positional and anisotropic temperature parameters of the non-hydrogen atoms, using SHELXL-97¹³. All the H atoms were positioned geometrically and constrained to ride on their parent atom with C—H = 0.93–0.97 Å and N—H = 0.86 Å, and with U_{iso}(H) = 1.5 U_{eq} for methyl H atoms and 1.2U_{eq}(C) for other H atoms. The components of the anisotropic displacement parameters in direction of the bond of C2, C3, C4 and C5 were restrained to be equal within an effective standard deviation of 0.001 using the DELU command. The general purpose crystallography tool PLATON¹⁴, ORTEP¹⁵ and MERCURY¹⁶ were used for structure analysis and presentation of the results.

2.3 Computational details

The molecular structure of the compound in ground state (in vacuo) was optimized using density functional theory (DFT) (B3LYP)^{17,18} method with the 6-311G (d, p)¹⁹ basis set. All the

calculations were performed without specifying any symmetry for the title molecule by using Gauss View molecular visualization program²⁰ and Gaussian 03 program package²¹. The optimized geometrical parameters, energy, atomic charges and dipole moments were calculated using Gaussian 03W package. GaussView 03 program has been used to construct optimized molecular geometry, Mullikan charges, HOMO, LUMO energy distributions and HOMO-LUMO energy gap^{22,23}.

3 Results and Discussion

3.1 Description of crystal structure

The displacement ellipsoid plot and theoretical geometry structure with the atom-numbering scheme for compound (1) is shown in Fig. 2. The compound (1) crystallizes as a colourless needle shaped in the monoclinic system, space group *C* 2/*c* with cell constants: $a = 18.6636(6)$ Å, $b = 9.8655(4)$ Å, $c = 19.5249(7)$ Å, $\alpha = \gamma = 90.0^\circ$, $\beta = 107.900(2)^\circ$, $V = 3421.0(2)$ Å³, $Z = 8$. Details of the data collection, crystal parameters and refinement process of compound (1) are given in Table 1.

The triazole (N1/N2/N3/C8/C9) ring is essentially planar [maximum deviation = 0.003(2) Å for the C8 atom] and forms dihedral angle of 7.21 (8)° with the pyrimidine ring. The phenyl ring attached to the pyrimidine ring is in axial position. The dihedral angle between the benzene rings is

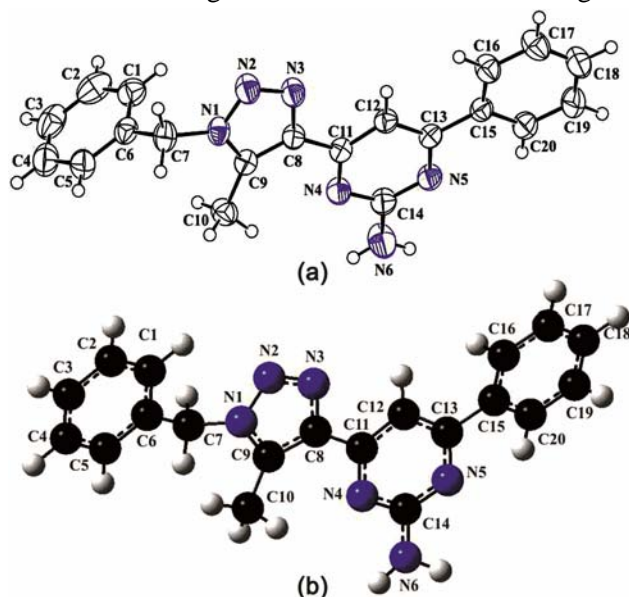


Fig. 2 — (a) View of title compound showing the atom-numbering scheme [displacement ellipsoids for the non-H atoms are drawn at the 50% probability level; H atoms are presented with spheres with arbitrary radii]; (b) Theoretical geometric structure of the title compound (B3LYP/6-311G(d,p)level)

80.42 (9)°. The bond distances N3—C8, C8—C9, C9—N1, N1—N2 and N2—N3 are 1.365(2), 1.382(2), 1.353(2), 1.355(2) and 1.300(2) Å, respectively, which agrees with C=C, N=N, C—N distances found in literature for compound having triazole heterocycles^{24,25}. In pyrimidine ring the N—C bond lengths [1.339(2) — 1.357(2) Å] and bond angles N6—C14—N5 [116.18(1)°] are found close to the reported values for similar pyrimidine derivatives²⁶.

The hydrogen bond geometry for compound (1) is presented in Table 2. The molecular conformation is stabilized by an intra-molecular C10—H10B...N4

Table 1 — Crystal and experimental data for the compound (1)

Empirical formula	C ₂₀ H ₁₈ N ₆
Formula weight	342.40
Temperature (K)	293(2)
Wavelength (Å)	0.71073
Crystal system	Monoclinic
Space group	<i>C</i> 2/ <i>c</i>
Unit cell dimensions(Å, °)	
<i>a</i>	18.6636(6)
<i>b</i>	9.8655(4)
<i>c</i>	19.5249(7)
β	107.90 (2)
Volume (Å ³)	3421.0(2)
<i>Z</i>	8
Calculated density (Mg m ⁻³)	1.330
Absorption coefficient (mm ⁻¹)	0.084
<i>F</i> (000)	1440
Crystal size (mm ³)	0.30 x 0.25 x 0.11
Theta range for data collection (°)	2.19 to 28.96.
Index ranges	-25 <= <i>h</i> <= 25, -13 <= <i>k</i> <= 13, -26 <= <i>l</i> <= 26
Reflections collected	19529
Independent reflections	4526 [R(int) = 0.0318]
Completeness to theta = 25.242°	99.8 %
Refinement method	Full-matrix least-squares on <i>F</i> ²
Data / restraints / parameters	4526 / 5 / 236
Goodness-of-fit on <i>F</i> ²	1.051
Final <i>R</i> indices [<i>I</i> > 2σ(<i>I</i>)]	R1 = 0.0495, wR2 = 0.1323
<i>R</i> indices (all data)	R1 = 0.0752, wR2 = 0.1505
Largest diff. peak and hole (e.Å ⁻³)	0.234 and -0.237.

Table 2 — Hydrogen bonding geometry for the compound (1) (Å, °)

D—H...A	D—H	d(H...A)	d(D...A)	<(DHA)
N6—H6A...N2 ⁱ	0.86	2.44	3.290(2)	172.6
C19—H19...Cg ⁱ	0.93	2.78	3.565(2)	142.0

Cg is the centroid of the C1—C6 ring.

Symmetry codes: (i) *x*, *I*-*y*, -*I*/*z* + *z*.

hydrogen bond, which generates an S(6) ring motif²⁷. In the crystal, molecules are linked into one-dimensional infinite chains along *c*-axis by N6—H6A...N2 hydrogen bonds and C19—H19...Cg1ⁱⁱⁱ interactions (Table 2 and Fig. 3; Symmetry code: (iii) = $x, 1-y, -1/2+z$, Cg1 is the centroid of the C1—C6 benzene ring). These chains are alternately connected along *a*-axis by centrosymmetrically π — π interactions with Cg2—Cg3^{iv} = 3.721(1) Å (Symmetry code: (iv) = $-x, 1-y, 1-z$) and Cg3—Cg4^v = 3.825(1) Å (Symmetry code: (v) = $1/2-x, 3/2-y, 1-z$) forming a two-dimensional supra-molecular network (Fig. 4; Cg2, Cg3 and Cg4 are the centroids of the triazole, pyrimidine and C15—C20 benzene rings, respectively).

3.2 DFT calculations

The first task for the computational work was to determine the optimized geometry of the title

compound. The starting coordinates were obtained from X-ray structure determination. The optimized parameters (bond lengths, bond angles) of the compound (1) were obtained using (DFT/B3LYP) method with the 6-311G(d,p) basis set. The results are listed in Table 3 and compared with the experimental data for the title compound.

As seen from the Table 3, the agreement between the theoretically calculated and the experimentally obtained structure parameters for the title compound are very good. In view of the bond lengths in Table 3, most predicted values are longer than experimental ones. It may be noted that the experimental results are for the solid phase and the theoretical calculations are for the gas phase. In the solid state, the existence of a crystal field along with the intermolecular interactions connect the molecules together, which results in the difference in bond parameters between the calculated and experimental values²⁸.

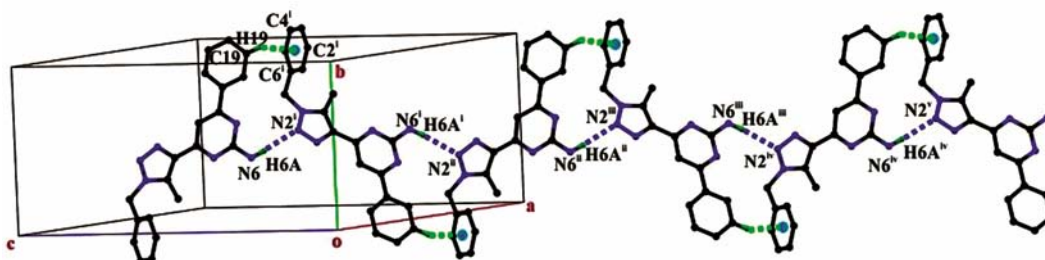


Fig. 3 — View of N6—H6A...N2 hydrogen bonds and C19—H19... π interactions forming one-dimensional infinite chains along *c*-axis [Cg is the centroid of the (C1—C6) benzene ring; {Symmetry code: (i) $x, 1-y, -1/2+z$; (ii) $x, y, -1+z$; (iii) $x, 1-y, -3/2+z$; (iv) $x, y, -2+z$; (v) $x, 1-y, -5/2+z$ }; hydrogen atoms not included in hydrogen bonding are omitted for clarity]

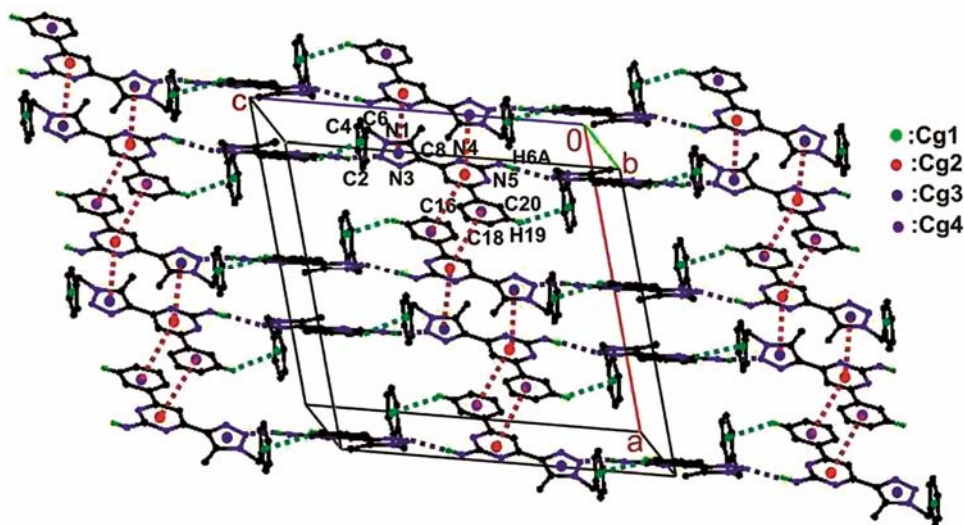


Fig. 4 — View of two-dimensional supramolecular network down the *a*-axis [N—H...N, C—H... π and π — π interactions are shown as blue, green and red dashed lines, respectively; Cg1, Cg2, Cg3 and Cg4 are the centroids of the (C1...C6) benzene ring, triazole, pyrimidine and (C15...C20) benzene ring, respectively; hydrogen atoms not included in hydrogen bonding are omitted for clarity]

Table 3 — Selected structural parameters by X-ray diffraction and DFT calculations for compound (1)

Parameters	X-ray	DFT
Bond lengths (Å)		
C1-C6	1.383(2)	1.3985
C2-C3	1.374(3)	1.3948
C3-C4	1.353(3)	1.3918
C4-C5	1.376(3)	1.3942
C5-C6	1.388(2)	1.3956
C8-N3	1.3651(2)	1.3684
C8-C9	1.382(2)	1.3903
C9-N1	1.3526(2)	1.3585
C9-C10	1.477(2)	1.49065
C11-N4	1.3371(2)	1.34062
C11-C12	1.383(2)	1.3974
C12-C13	1.3845(2)	1.3964
Bond angles (°)		
C4-C5-C6	121.23(2)	119.178
C1-C6-C5	118.46(2)	119.178
C1-C6-C7	121.71(2)	120.442
C5-C6-C7	119.82(1)	120.354
N1-C7-C6	113.20(1)	113.705
N3-C8-C9	108.77(1)	108.346
N3-C8-C11	119.97(1)	120.777
C9-C8-C11	131.25(1)	130.877
N1-C9-C8	103.38(1)	103.395
N1-C9-C10	123.12(1)	123.349
C11-C12-C13	118.11(1)	117.436
N5-C14-N4	127.31(1)	126.725
N5-C14-N6	116.18(1)	116.558
N4-C14-N6	116.51(2)	116.706
N2-N3-C8	109.26(1)	109.645
C11-N4-C14	114.97(1)	115.967
Torsion angles (°)		
N5-C13-C15-C16	176.31(1)	164.009
C12-C13-C15-C16	-2.0(2)	-16.613
N5-C13-C15-C20	-2.88(2)	-15.743
C12-C13-C15-C20	178.84(1)	163.635
C6-C7-N1-C9	61.9(2)	77.618

When the X-ray structure of the title compound is compared with its optimized counterpart (Fig. 2), conformational discrepancies are observed. The orientation of the phenyl ring of compound (1) proved the most notable discrepancy and is defined with torsion angle $N5-C13-C15-C20 = -2.88(2)^\circ$, which is calculated at -15.743° for B3LYP/6-311G (d,p) level. As seen from Table 3, the difference between the X-ray and calculated values for the bond lengths C3-C4, C19-C18 and N6-C14 are 0.0388 Å, 0.022 Å and 0.0123, respectively. Similarly, the difference for bond angles C11-N4-C14, C1-C6-C7 and C4-C5-C6 are 1.0° , 1.268° and 2.052° , respectively. This difference is more not only because of intra-molecular C10-H10B...N4 hydrogen bond but also due to intermolecular

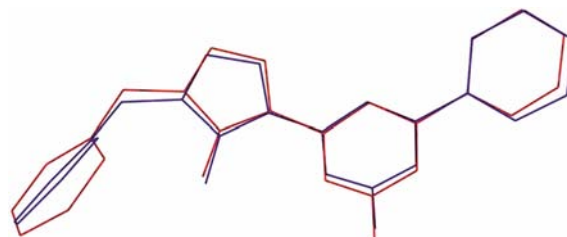


Fig. 5 — Atom-by-atom super-imposition of the calculated structure (blue) and the X-ray structure (red) for compound (1)

N6-H6A...N2 and C-H... π interactions. According to experimental and theoretical values, the dihedral angles between triazole and pyrimidine rings are $7.21(8)^\circ$ and 2.67° , respectively and also between benzene rings are $80.42(9)^\circ$ and 85.93° , respectively.

A global comparison was performed by superimposing the molecular skeletons obtained from X-ray diffraction and the theoretical calculations atom by atom (Fig. 5), obtaining RMSE's values of 0.443 Å for (DFT/B3LYP) method with the 6-311G(d,p) basis set. This magnitude of RMSE can be explained by the fact that the intermolecular columbic interaction with the neighbouring molecules are absent in gas phase, whereas the experimental result corresponds to interacting molecules in the crystal lattice.

3.3 Mulliken analysis

The atomic charge in molecules is fundamental to chemistry. For instance, atomic charge has been used to describe the processes of electro-negativity equalization and charge transfer in chemical reactions^{29,30} and to model the electrostatic potential outside molecular surfaces³¹⁻³³. Mulliken atomic charges calculated at the B3LYP/6-311G(d,p) methods are collected in Table 4. Illustration of atomic charges plotted at 6-311G (d,p) level has been shown in Fig. 6. It is worthy to mention that C14, C13, C11, and C9 atoms of title compound exhibit positive charges, while other carbon atoms exhibit negative charges. The charge values for Nitrogen N4 and C10 atoms are -0.4175 and -0.2502 a.u., respectively. The positive atomic charge is obtained for H10B is 0.1438 a.u. However, all the hydrogen atoms exhibit a net positive charge. The presence of large negative charge on N4 and C10 atoms and net positive charge on H10B atom may confirms the formation of C10-H10B...N4 intra-molecular interaction in solid forms.

Table 4 — Mulliken atomic charges of compound (1)

Atom	Atomic charge
N1	-0.3275
N2	-0.0322
N3	-0.2439
N4	-0.4175
N5	-0.4003
N6	-0.4660
C1	-0.0445
C2	-0.0908
C3	-0.0846
C4	-0.0922
C5	-0.0711
C6	-0.1322
C7	-0.0139
C8	-0.0604
C9	0.2800
C10	-0.2503
C11	0.1314
C12	-0.0450
C13	0.1627
C14	0.4464
C15	-0.1193
C16	-0.0582
C17	-0.1017
C18	-0.0778
C19	-0.0959
C20	-0.0133
H1	0.1126
H2	0.1018
H3	0.0994
H4	0.0976
H5	0.0871
H6A	0.2227
H6B	0.2205
H7A	0.1269
H7B	0.1596
H10A	0.1366
H10B	0.1438
H10C	0.1185
H12	0.1111
H16	0.1001
H17	0.0939
H18	0.0940
H19	0.0939
H20	0.0980

3.4 Molecular orbital studies

The most widely used theory by chemists is the molecular orbital (MO) theory. The frontier molecular orbitals play an important role in the electronic and optical properties as well as in UV-VIS spectra and chemical reactions³⁴. The DFT calculated

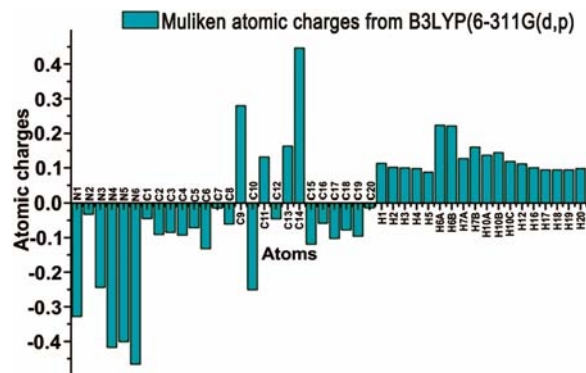


Fig. 6 — Bar diagram representing the charge distribution of compound (1)

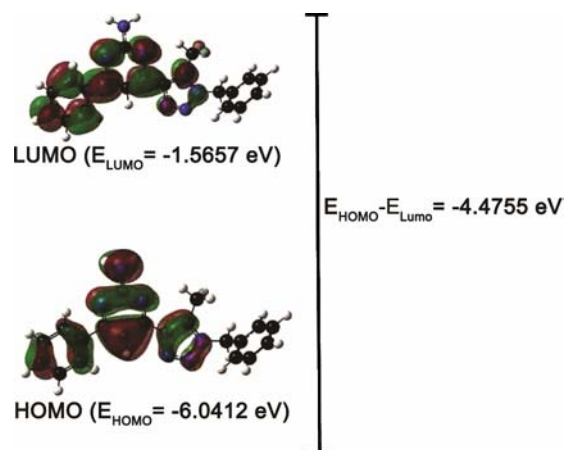


Fig. 7 — Molecular orbital and energies for the HOMO and LUMO of compound (1)

electronic absorption spectra, the maximum absorption wavelength corresponding to the electronic transition is from the highest occupied molecular orbital (HOMO) to the lowest unoccupied molecular orbital (LUMO). The frontier molecular orbital energies of the title compound are shown in Fig. 7.

The energy gap between HOMO and LUMO is a critical parameter in determining molecular electrical transport properties^{35,36}. The lowest unoccupied molecular orbital (LUMO) energy is -1.5657 eV and the highest occupied molecular orbital (HOMO) energy is -6.0412 eV. The energy gap of HOMO–LUMO explains the ultimate charge transfer interaction within the molecule and the frontier orbital energy gap of title compound is found to be -4.4755 eV obtained at DFT method using 6-311G(d,p) basis set. Lower HOMO–LUMO gap explains the eventual charge transfer interactions taking place within the molecule, which influences the biological activity of the molecule.

3.5 Chemical reactivity

Chemical reactivity indices like chemical hardness (η), electro-negativity (χ), electronic chemical potential (μ), and electro-philicity Index (ω), are calculated using DFT. Chemical hardness is associated with the stability and reactivity of a chemical system. In a molecule, it measures the resistance to change in the electron distribution or charge transfer. On the basis of frontier molecular orbitals, chemical hardness corresponds to the gap between the highest occupied molecular orbital (HOMO) and lowest unoccupied molecular orbital (LUMO). Chemical hardness is approximated using equation $\eta = (E_{\text{LUMO}} - E_{\text{HOMO}})/2$, where E_{LUMO} and E_{HOMO} are the LUMO and HOMO energies, respectively. The larger the HOMO–LUMO energy gap, the molecule will be harder, more stable and less reactive. Table 5 contains the computed chemical hardness value for title compound.

The concept of electro-negativity put forward by Pauling³⁷ is defined as the power of an atom in a molecule to attract electrons towards it. Higher is the electro-negativity of the species, greater is its electron accepting power or rather the electro-philicity. Electro-negativity is determined using equation $\chi = - (E_{\text{HOMO}} + E_{\text{LUMO}}) / 2$, Table 5 contains the computed electro-negativity values for title compound.

Electronic chemical potential is defined as the negative of electro-negativity of a molecule³⁸ and determined using equation $\mu = (E_{\text{HOMO}} + E_{\text{LUMO}})/2$. Physically, μ describes the escaping tendency of electrons from an equilibrium system³⁹. The value of μ for title compound is presented in Table 5.

Global electro-philicity index (ω), introduced by Parr, is calculated using the electronic chemical potential and chemical hardness as shown in equation $\omega = \mu^2/2\eta$. Electro-philicity index measures the propensity or capacity of a species to accept electrons^{40,41}. It is a measure of the stabilization

in energy after a system accepts additional amount of electronic charge from the environment^{42,43}. The electro-philicity values of the title compound is presented in Table 5.

The HOMO and LUMO orbital energies are related to gas phase ionization energies (I) and electron affinities (A) of the isomers according to the Koopmans' theorem through equations $A = - E_{\text{LUMO}}$, $I = - E_{\text{HOMO}}$. Electron affinity refers to the capability of a ligand to accept precisely one electron from a donor.

3.6 Molecular electrostatic potential

The molecular electrostatic potential (MEP) is a plot of electrostatic potential mapped onto the constant electron density surface. The MEP has been used primarily for predicting sites and relative reactivity towards electro-philic attack, in studies of biological recognition and hydrogen bonding interactions^{44,45}. The negative electrostatic potential corresponds to an attraction of the proton by the concentrated electron density in the molecule (and is coloured in shades of red on the EPS surface), the positive electrostatic potential corresponds to repulsion of the proton by atomic nuclei in regions where low electron density exists and the nuclear charge is incompletely shielded (and is coloured in shades of blue). Potential increases in the order red < orange < yellow < green < blue.

Figure 8 shows the molecular electrostatic potential (MEP) and was determined using B3LYP/6-311G(d, p) method. The different values of the electrostatic potential at the surface are represented by different colours. As can be seen in Fig. 8, the negative (red) region is localized on the un-protonated atom of N2, with a minimum value -0.048 a.u. However, positive (blue) region is localized on atom N6

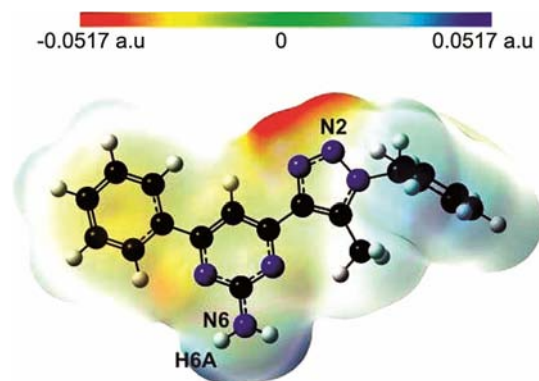


Fig. 8 — Molecular electrostatic potential map calculated using B3LYP/6-311G(d, p) level

Table 5 — Calculated energy values of compound (1) by B3LYP/6-311G(d,p)

Basis set	B3LYP/6-311G(d,p)
E_{HOMO} (eV)	-6.0412
E_{LUMO} (eV)	-1.5655
$E_{\text{HOMO}} - E_{\text{LUMO}}$ gap (eV)	-4.4755
Chemical hardness (η)	2.2378
Chemical potential (μ)	-3.8035
Electro-negativity (χ)	3.8035
Electro-philicity index (ω)	3.2323

Table 6 — Thermodynamical parameters of compound (1) by B3LYP/6-311G(d,p)

Parameter	Value (at 298 K)
Total energy (Hartree)	-1101.75
Zero point energy (K cal mol ⁻¹)	219.75873
Rotational constants (GHz)	0.46868 0.08071 0.07502
Entropy (cal.mol ⁻¹ K ⁻¹)	
Total	162.352
Translational	43.416
Rotational	35.999
Vibrational	82.937
Dipole moment (Debye)	4.3217

Table 7 — Thermodynamic properties of compound (1) at different temperatures at B3LYP/6-311G(d,p) level

Temperature (K)	C _{p,m} ^o (cal.mol ⁻¹ K ⁻¹)	S _m ^o (cal.mol ⁻¹ K ⁻¹)	H _m ^o (Kcal.mol ⁻¹)
100	33.343	101.370	221.872
200	57.572	133.121	226.392
300	84.736	162.352	233.494
400	111.085	190.979	243.309
500	133.561	218.707	255.579

probably due to hydrogen, with a value 0.041 a.u. Therefore, Fig. 7 confirms the existence of an intermolecular N6–H6A...N2 interactions.

3.7 Thermodynamic properties

The thermodynamics parameters of the compound have also been computed in order to get reliable relations among energetic, structural and reactivity characteristics of the molecules. Knowledge of permanent dipole moment of a molecule allows to determine molecule's conformation.

The values of thermodynamic parameters such as zero-point vibration energy, thermal energy and dipole moment of title compound by DFT method with 6-311G(d,p) basis set at 298.15 K and 1 atm pressure were calculated and listed in Table 6. From Table 6, the high value of dipole moment of title compound signifies high delocalization of charges, resulting in the formation of relatively loose structured, charge separated species.

The temperature dependence of the thermodynamic properties such as heat capacity at constant pressure (C_{p,m}^o), entropy (S_m^o) and enthalpy (H_m^o) for the title compound have been determined by B3LYP/6-311G(d,p) method in temperature range 100-500 K and listed in Table 7. From Table 7, it can be

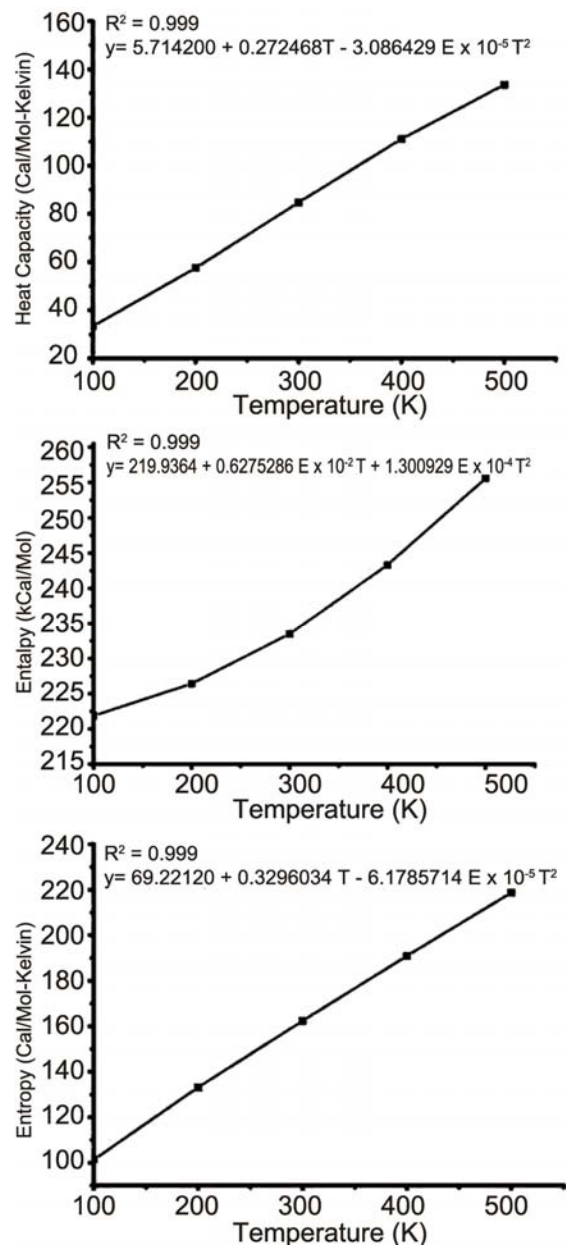


Fig. 9 — Variation of thermodynamic parameters with temperature for compound (1)

observed that these thermodynamic parameters increase with rise of temperature due to the fact that the molecular vibration thermal energies increase with temperature. The correlation equations between heat capacities, entropies, enthalpy changes and temperatures were fitted by quadratic formulas given in equations. Below and the corresponding fitting factors (R²) for these thermodynamic properties were found to be 0.999. The temperature dependence correlation graphs are shown in Fig. 9.

$$C_{p,m}^{\circ} = 5.714200 + 0.272468 T - 3.086429 E \times 10^{-5} T^2$$

$$(R^2 = 0.999)$$

$$S_m^{\circ} = 69.22120 + 0.3296034 T - 6.1785714 E \times 10^{-5} T^2$$

$$(R^2 = 0.999)$$

$$H_m^{\circ} = 219.9364 + 0.6275286 E \times 10^{-2} T + 1.300929 E \times 10^{-4} T^2$$

$$(R^2 = 0.999)$$

These equations could be used for further studies on the title compound. For instance, when the interaction of title compound with another compound is studied, these thermodynamic properties could be obtained from the above equation and then can be used to calculate the change in Gibbs free energy of the reaction, which will in turn help to judge the spontaneity of the reaction.

4 Conclusions

The title compound (1) was synthesized and has been confirmed by NMR and structural (single-crystal X-ray diffraction) techniques. To support the solid state structure, the geometric parameters of the title compound have been calculated using density functional theory DFT (B3LYP) method with the 6-311G(d, p) basis sets, and compared with the experimental findings. It is noted here that the experimental results belong to solid phase and theoretical calculations belong to gaseous phase. In the solid state, the existence of the crystal field along with the intermolecular interactions have connected the molecules together, which result in the differences of bond parameters between the calculated and experimental values. The small HOMO-LUMO gap value shows that the molecule is biologically active. The MEP map shows that the negative potential sites are on nitrogen atom as well as the positive potential sites are around the hydrogen atoms and hence, MEP map confirms the existence of intermolecular N–H...N interaction. The calculated HOMO and LUMO energies can be used to semi-quantitatively estimate the ionization potential, electron affinity, electro-negativity, electro-philicity index, hardness, and chemical potential. The correlations between the statistical thermodynamics and temperature are also obtained. It is seen that the heat capacities, entropies and enthalpies increase with the increasing temperature owing to the intensities of the molecular vibrations increase with increasing temperature.

Supplementary materials

CCDC987426 contains the supplementary crystallographic data for this paper. This data can be obtained free of charge at http://www.ccdc.cam.ac.uk/data_request/cif, by e-mailing data_request@ccdc.cam.ac.uk, or by contacting The Cambridge Crystallographic Data Centre, 12 Union Road, Cambridge CB21EZ, UK; fax: +44(0)1223-336033.

Acknowledgement

The authors thank Dr Babu Vargheese, SAIF, IIT, Madras, India, for his help with the data collection.

References

- Morales-Sanfrutos J, Ortega-Munoz M, Lopez-Jaramillo J, Hernandez-Mateo F & Santoyo-Gonzalez F, *J Org Chem*, 73 (2008) 7768.
- Genin M J, Allwine D A, Anderson D J, Barbachyn M R, Emmert D E, Garmon S A, Graber D R, Grega K C, Hester J B, Hutchinson D K, Morris J, Reischer R J, Ford C W, Zurenko G E, Hamel J C, Schaadt R D, Stapert D & Yagi B H, *J Med Chem*, 43 (2000) 953.
- Buckle D R, Rockell C J M, Smith H & Spicer B A, *J Med Chem*, 29 (1986) 2262.
- Giffin M J, Heaslet H, Brik A, Lin Y C, Cauvi G, Wong C H, McRee D E, Elder J H, Stout C D & Torbett B E, *J Med Chem*, 51 (2008) 6263.
- Wang S, Wang Q, Wang Y, Liu L, Weng X, Zhang G L X & Zhou X, *Bioorg Med Chem Lett*, 18 (2008) 6505.
- El-Subbagh H I, Abu-Zaid S M, Mahran M A, Badria F A, Al-Obaid A M, *J Med Chem*, 43 (2000) 2915.
- Trivedi A R, Dodiya D K, Ravat N R & Shah V H, *Arkivoc*, 6 (2008) 131.
- Koch W & Holthausen M C A, *A Chemistry guide to density functional theory* (Wiley-VCH, Weinheim, New York, Chichester), 2000.
- Parr R G & Yang W T, *Density functional theory of atoms and molecules* (Oxford University Press, New York), 1989.
- Nagarajan S, Shanmugavelan P, Sathishkumar M, Selvi R, Ponnuswamy A, Harikrishnan H & Shanmugaiah V, *Chin Chem Lett*, 25 (2014) 419.
- Bruker, *APEX-II & SAINT-Plus (Version 7.06a)* (Bruker AXS Inc, Madison, Wisconsin, USA), 2004.
- Farrugia L J, *J Appl Cryst*, 32 (1999) 837.
- Sheldrick G M, *Acta Cryst*, 64 (2008) 112.
- Spek A L, *J Appl Cryst*, 36 (2003) 7.
- Farrugia L J, *J Appl Cryst*, 30 (1997) 565.
- Bruno I J, Cole J C, Edgington P R, Kessler M, Macrae C F, McCabe P, Pearson J & Taylor R, *Acta Cryst*, 58 (2002) 389.
- Becke A D, *J Chem Phys*, 98 (1993) 648.
- Lee C, Yang W & Parr R G, *Phys Rev B*, 37 (1988) 785.
- Ditchfield R, Hehre W J & Pople J A, *J Chem Phys*, 54 (1971) 724.
- Dennington R II, Keith T & Millam J, *GaussView (Version 4.1.2.)* (Semichem Inc., Shawnee Mission), 2007.
- Frisch M J, Trucks G W, Schlegel H B, Scuseria G E, Robb M A, Cheeseman J R, Montgomery J A, Vreven T, Kudin K N, Burant J C, Millam J M, Iyengar S S, Tomasi J, Barone V,

- Mennucci B, Cossi M, Scalmani G, Rega N, Petersson G A, Nakatsuji H, Hada M, Ehara M, Toyota K, Fukuda R, Hasegawa J, Ishida M, Nakajima T, Honda Y, Kitao O, Nakai H, Klene M, Li X, Knox J E, Hratchian H P, Cross J B, Adamo C, Jaramillo J, Gomperts R, Stratmann R E, Yazyev O, Austin A J, Cammi R, Pomelli C, Ochterski J W, Ayala P Y, Morokuma K, Voth G A, Salvador P, Dannenberg J J, Zakrzewski V G, Dapprich S, Daniels A D, Strain M C, Farkas O, Malick D K, Rabuck A D, Raghavachari K, Foresman J B, Ortiz J V, Cui Q, Baboul A G, Clifford S, Cioslowski J, Stefanov B B, Liu G, Liashenko A, Piskorz P, Komaromi I, Martin R L, Fox D J, Keith T, Al-Laham M A, Peng C Y, Nanayakkara A, Challacombe M, Gill P M W, Johnson B, Chen W, Wong M W, Gonzalez C & Pople J A, *Gaussian 03, Revision B 05* (Gaussian Inc, Pittsburgh), 2004.
- 22 Frisch A E, Nielsen A B & Holder A J, *Gaussview* (Gaussian Inc, Pittsburgh), 2003.
- 23 Young D C, *Computational chemistry: A practical guide for applying techniques to real-world problems (Electronics)* (John Wiley Sons Inc, New York), 2001.
- 24 Huang C C, Wu F L, Lo Y H, Lai W R & Lin C H, *Acta Cryst*, 66 (2010) 1690.
- 25 Sarmiento-Sánchez J I, Aguirre G & Rivero I A, *Acta Cryst*, 67 (2011) 1856.
- 26 Bukhari Mujahid Hussain, Siddiqui Hamid Latif, Chaudhary Muhammad Ashraf, Hussaina Tanvir & Parvez Masood, *Acta Cryst*, 64 (2008) 963.
- 27 Bernstein J, Davis R E, Shimoni L & Chang N L, *Angew Chem Int Ed Engl*, 34 (1995) 1555.
- 28 Jian F F, Zhao P S, Bai Z S & Zhang L, *Struct Chem*, 16 (2005) 635.
- 29 Jug K & Maksic Z B, In *Theoretical model of chemical bonding* (Springer, Berlin), 1991.
- 30 Fliszar S, *Charge distributions and chemical effects* (Springer, Berlin, Heidelberg, New York), 1983.
- 31 Smith P E & Montgomery Pettitt B, *J Am Chem Soc*, 113 (1991) 6029.
- 32 Gao J, *J Chem Phys*, 98 (1993) 1975.
- 33 Cieplak P & Kollman P, *J Comput Chem*, 12 (1991) 1232.
- 34 Fleming I, *Frontier orbitals and organic chemical reactions* (Wiley, London), 1976.
- 35 Fukui K, *Science*, 218 (1982) 747.
- 36 Udhayakala P, Rajendiran T V, Seshadri S & Gunasekaran S, *J Chem Pharm Res*, 3 (3) (2011) 610.
- 37 Pauling L, *The nature of chemical bond* (Cornell University Press, Ithaca), 1960.
- 38 Parr R G & Pearson R G, *J Am Chem Soc*, 105 (1983) 7512.
- 39 Chattaraj P K & Maiti B, *J Am Chem Soc*, 125 (2003) 2705.
- 40 Vektariene A, Vektaris G & Svoboda J, *Arkivoc*, 7 (2009) 311.
- 41 Parr R G, Szentpaly L & Liu S, *J Am Chem Soc*, 121 (1999) 1922.
- 42 Koopmans T, *Physica*, 1 (1933) 104.
- 43 Liu S, *J Chem Sci*, 117 (2005) 477.
- 44 Murray J S & Sen K, *Molecular electrostatic potentials: Concepts and applications* (Elsevier, Amsterdam), 7 (1996) 624.
- 45 Scrocco E & Tomasi J, *Adv Quant Chem*, 11 (1978) 115.